SANDIA REPORT
SAND2005-7644
Unlimited Release
Printed June 2007

Infiltration in Unsaturated Layered Fluvial Deposits at Rio Bravo: Photo Essay and Data Summary

James R Brainard, Robert J Glass

Prepared by
Sandia National Laboratories
Albuquerque, New Mexico 87185 and Livermore, California 94550

Sandia is a multiprogram laboratory operated by Sandia Corporation,
a Lockheed Martin Company, for the United States Department of Energy's
National Nuclear Security Administration under Contract DE-AC04-94AL85000.

Issued by Sandia National Laboratories, operated for the United States Department of Energy by Sandia Corporation.

SAND2005-7644
Unlimited Release
Printed August 2007

Infiltration in Unsaturated Layered Fluvial Deposits at Rio Bravo: Photo Essay and Data Summary

JR Brainard, RJ Glass
Flow Visualization and Processes Laboratory
Sandia National Laboratories

Abstract

An infiltration and dye transport experiment was conducted to visualize flow and transport processes in a heterogeneous, layered, sandy-gravelly fluvial deposit adjacent to Rio Bravo Boulevard in Albuquerque, NM. Water containing red dye followed by blue-green dye was ponded in a small horizontal zone (~0.5 m x 0.5 m) above a vertical outcrop (~4 m x 2.5 m). The red dye lagged behind the wetting front due to slight adsorption thus allowing both the wetting front and dye fronts to be observed in time at the outcrop face. After infiltration, vertical slices were excavated to the midpoint of the infiltrometer exposing the wetting front and dye distribution in a quasi three-dimensional manner. At small-scale, wetting front advancement was influenced by the multitude of local capillary barriers within the deposit. However at the scale of the experiment, the wetting front appeared smooth with significant lateral spreading ~ twice that in the vertical, indicating a strong anisotropy due to the pronounced horizontal layering. The dye fronts exhibited appreciably more irregularity than the wetting front, as well as the influence of preferential flow features (a fracture) that moved the dye directly to the front, bypassing the fresh water between.

Acknowledgment

This experiment was conducted as part of a Vadose Zone class project taught by RJ Glass at the University of New Mexico in early spring of 1992. Class participants included: Karl Martin, Drew Baird, Jim Brainard, Bob Holt, Dan Garrett, and Rick Morris. Portions of this field experiment were reported in Martin et al., [1993] and Glass and Nicholl [1996] as well as at many national scientific meetings since 1992. We acknowledge funding from the Department of Energy (DOE) Environmental Management and Science Program under contracts DE-AC04-94 AL85000 to Sandia National Laboratories for the analysis of the data and preparation of the manuscript.

Contents

List of Tables

List of Figures

1. Introduction

During the past two decades, numerous field infiltration and tracer experiments (e.g., Wierenga, et al., 1986; Sisson and Lu, 1984; Gee and Ward, 2001; Brainard, 1997; Brainard et al., 2004a) have been conducted to study infiltration and solute transport processes in the heterogeneous vadose zone. Monitoring the processes in these field experiments has mainly relied on measurements of capillary pressure, moisture content, and tracer concentration using tensiometers, neutron access tubes, and suction lysimeters over a large area. As a consequence these sparse measurements depict moisture and solute distributions only at low spatial resolution. Recent advanced geophysical surveys (such as cross-borehole ground penetrating radar and electric resistivity tomography) are making the imaging of these distributions in multi-dimensions possible. Spatial resolution of these geophysical measurements, however, is limited and their ability to accurately detect moisture content and solute concentration remains to be fully assessed (e.g., Alumbaugh et al., 2002; Yeh et al., 2002; Binley, et al., 2001).

Here, we present a photo essay of a simple but unique field infiltration experiment designed to provide detailed photographic documentation of flow and transport processes occurring during water infiltration in a heterogeneous fluvial deposit with significant layering. The experiment involved infiltrating water containing slightly adsorbing dye tracers immediately above a vertical outcrop in the sandy-gravelly fluvial deposit at Rio Bravo Boulevard in Albuquerque, New Mexico just east of Interstate 25. Infiltration of dyes above a vertical outcrop allowed documentation of the spatial-temporal evolution of both the wetting and lagging dye fronts on the face of the outcrop as infiltration progressed. Subsequent excavation of the outcrop in a series of vertical slices back from the face allowed for a quasi three-dimensional visualization of the dye and wetting front structure. The photographic record captures the spatial evolution of the infiltrated dyes and water at both the outcrop and microlayer scales.

The Rio Bravo infiltration experiment was performed as part of a graduate level Vadose Zone Hydrology class at the University of New Mexico during the Spring semester of 1992. Due to budgetary constraints we looked for a location where we could undertake an experiment with minimal costs. We were fortunate to find the Rio Bravo site because not only was the outcrop exposed in a road cut which made hand excavation possible, but the outcrop also displayed complex sedimentary structures common to fluvial deposits found worldwide.

This photo essay complements a paper by Glass et al. (2004) where a brief description of the experimental design is presented along with a subset of photographs depicting both the experimental setup and development of the colorful bulb on the outcrop and excavated slices. In this photo essay, we provide a complete photographic documentation of the experimental design, setup and results.

This page intentionally left blank.

2. Field Experiment

The experimental site was located 0.1 mile east of I-25 on the south side of Rio Bravo Boulevard (Figure 2.1). The site is located on fluvial deposits within the Neogene/Quaternary Santa Fe Group, which comprise the principal fill of the Albuquerque Basin; one of the largest of a series of eastward stepping, en-echelon structural basins within the Rio Grande Rift [Kelley, 1977; Hawley, 1978]. Topographic expression of the Rio Grande Rift is apparent in Figure 2.1. In central and northern New Mexico the Rio Grande (Big River in English) flows within the narrow valley delineating the Rio Grande Rift basins while in the south the rift merges with the larger basin and range province.

2.1 Site location and description

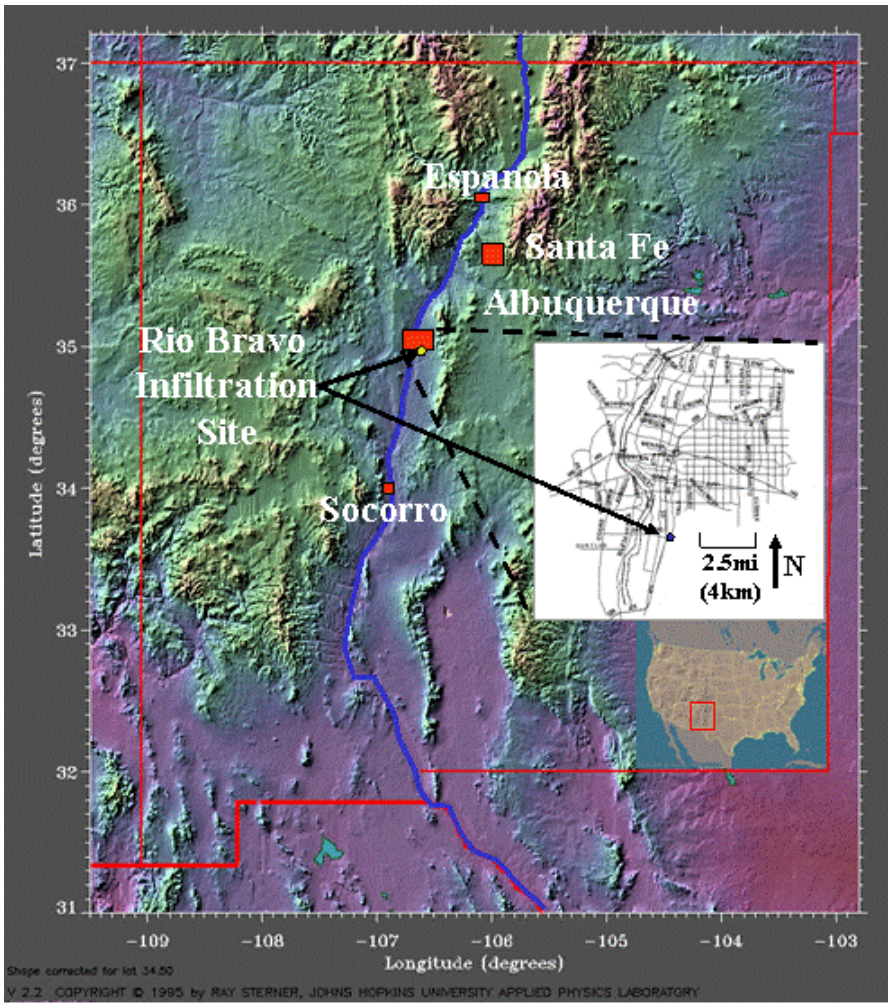

Figure 2.1: The Rio Bravo Infiltration site was located on the south side of Albuquerque, New Mexico. This Color enhanced composite satellite image of the State of New Mexico shows Albuquerque relative to other notable New Mexico cities such as Socorro, Espanola and of course Santa Fe. An inset map shows the location of the Rio Bravo Vadose Zone Infiltration Facility relative to the major cross streets in Albuquerque.

Figure 2.2: View of the Rio Bravo Infiltration Site from the north across Rio Bravo Boulevard. Exposed in the outcrop is a sandy-gravely fluvial deposit within the upper Santa Fe Group; an extensive basin fill deposit within the Rio Grand Rift. Albuquerque International Airport is due east of the Rio Bravo Site. In this photo, much of the experimental apparatus is in place. The outcrop is approximately 2 meters high and consists of ancestral Rio Grande bedded sand and gravel deposits. Bob Glass is seen kneeling to the left of the infiltrometer where he is negotiating working conditions with the graduate students. Notice the camera mounted on the orange ladder behind the blue truck and the garbage can used as a supply tank for the infiltrometer. Notice also the Bob Glass Bomb, the grey Oldsmobile to the left of the blue truck. This vehicle is a remnant of Bob's graduate school days that he had a hard time giving up…until the car gave it up.

Figure 2.3: A series of views of the Rio Bravo spanning southwest to the west showing nearby industrial areas of the South Valley. The proximity of the Rio Bravo site to the industrial areas is a reminder of the potential practical application that field infiltration studies can have. Results from infiltration experiments can provide a better understanding of vadose zone flow and transport processes which can be used to test and revise existing conceptual models and provide the foundation for developing new models that accurately reflect underlying flow and transport processes, the desired end result being the implementation of cost effective and technically efficient monitoring and remediation practices.

2.2 Geology

Understanding the hydrology of a region requires knowledge of the geology. This is especially true in the vadose zone where water flows mostly in the unsaturated state and geologic heterogeneities can have a remarkable impact on the velocity and direction of water and contaminants flow. Therefore, we present in some detail the geology of the Rio Bravo site to provide a foundation for interpreting the results of this experiment.

The fluvial sediments at the Rio Bravo Infiltration site were mapped into 5 macro units having similar texture and structures and bounded by erosional contacts. The units are predominantly weakly cemented and non- to slightly friable, except for the upper unit (Unit 5), which has moderately strong cementation forming a resilient cap on the outcrop. Starting at the bottom, Unit 1 is a fine to coarse-grained sandstone and is bounded above by a pebble-granule conglomerate (Unit 2). Unit 3 is a medium to coarse-grained sandstone capped by the fine to medium-grained sands of Units 4. Unit 5, the topmost unit in the outcrop, is also a fine to medium grained sand but lacks pebble gravel inter-beds as observed in Unit 4. Of all the units, Unit 5 is most indurated and forms an erosion resistant and very likely a low permeability cap over the outcrop. Within each unit, well developed laminations and cross-bedding with thickness on the order of millimeters to centimeters were observed. Table 2.1 gives a more complete description of each of these units.

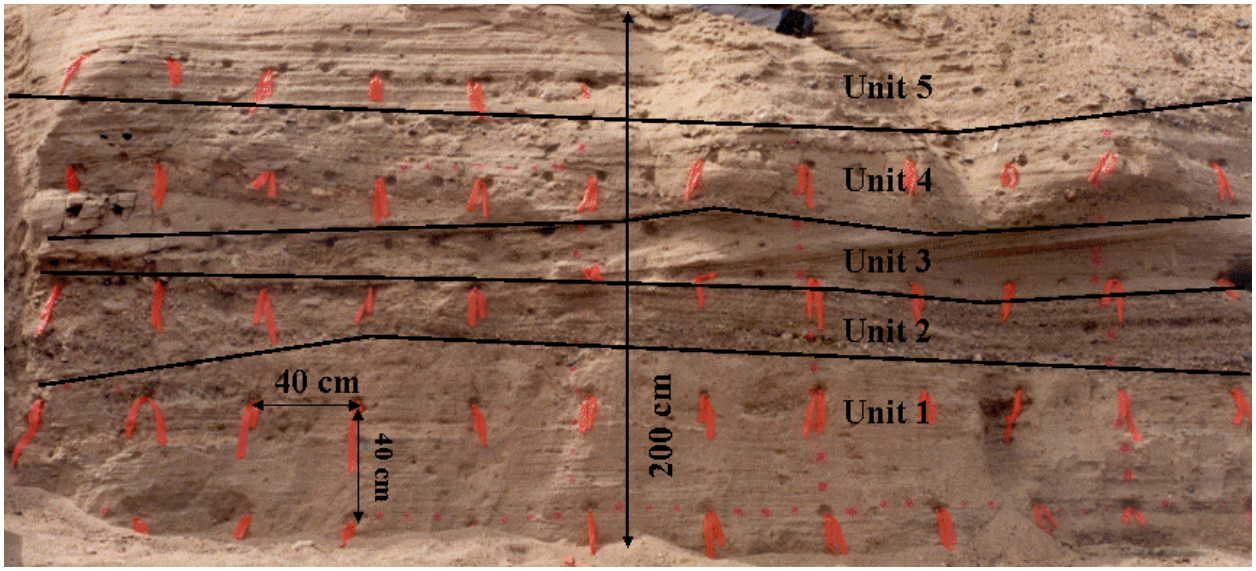

Figure 2.4: Close-up view of the outcrop seen in the distance in Figure 2.2 delineating geologic units. The orange flags provided a 40 by 40 cm reference grid.

Table 2.1. Geologic Description of Geologic Units

NOTE: Units are listed in ascending order, from outcrop base to the outcrop cap

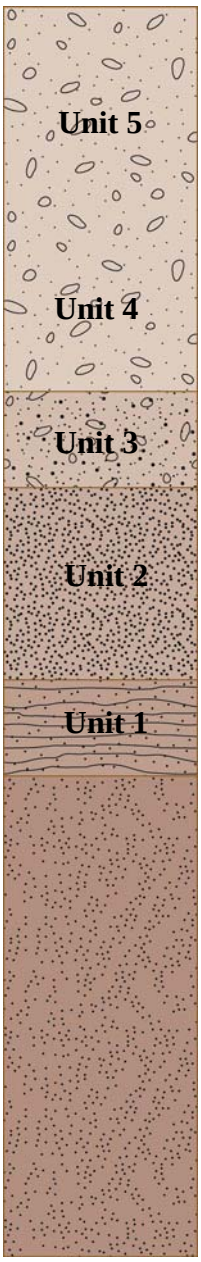

Unit 5: A fine-to medium grained, moderately-cemented sandstone.
Average thickness 60 cm
Planar and parallel thin laminae and thin beds with occasional lag pebbles
Low angle cross-cutting relationships are rare
Upper contact is not exposed in the outcrop

Unit 4: A fine to medium grained, weakly-cemented, slightly-friable sandstone.
Average thickness: 15 cm
Thin to very thin planer laminae with local interbeds of pebble/granule conglomerate
Laminae are mostly parallel but locally display low angle cross-cutting relationships
Cobble-sized rip-up clasts of sandstone and mudstone occur near the base
Upper contact is picked at the top of a bedding plane above which pebble/granule interbeds are not present

Unit 3: A fine to medium grained, weakly cemented, slightly-friable sandstone.
Average thickness: 30 cm
Thinly laminated to laminated with local pebble and granule lags
Strata are parallel and planer with abundant low-angle tangential cross-stratification
Coarse to very coarse sand with granules occurs locally; pebble lags cap some erosional surfaces on the left side of the out crop
Carbonate cement concentrated at tops of strata
Upper contact is located at the sharp textural transition to Unit 4

Unit 2: A pebble-granule weakly cemented, slightly-friable conglomerate with pebbles and granules in a matrix of medium to coarse sandstone.
Average thickness: 15 cm
Strata are laminae-scale, planer and parallel with low-angle cross-cutting relationships; some local tangential cross-laminae are also present
Upper contact is located at the sharp textural transition to the Unit 3 sandstone

Unit 1: A fine to coarse, weakly-cemented, non friable sandstone.
Average exposed thickness: 75 cm
Lower contact not exposed
Horizontal to subhorizontal carbonate indurated thin laminae
Strata are mostly parallel with some low-angle cross-cutting relationships
Carbonate cement is most abundant in the finer grained fractions near the top of the each stratum
Sorted to poorly sorted fine sand at base and poorly sorted coarse sand and granules near the top
Fining-upward sequences are present in the upper part of the unit
Local zones of soft sediment deformation present along the left edges of the outcrop as viewed in **Figure 1.**

Figure 2.5: Close-up view of the Rio Bravo infiltration site outcrop. The heterogeneous nature of the upper two thirds of the outcrop is highlighted by differential erosion exhibited in this view. Loose debris was removed from the lower third of the outcrop to expose undisturbed sediments. A yardstick provides scale.

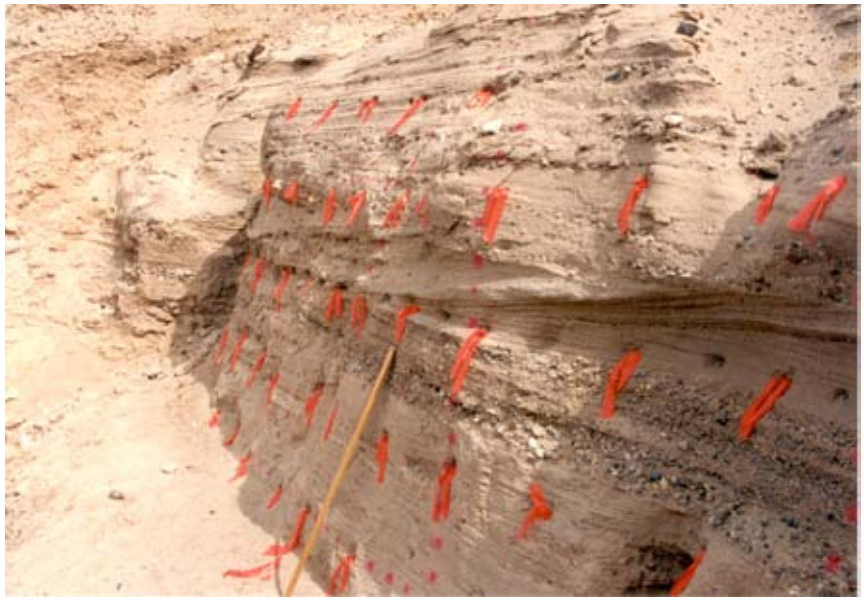

Figure 2.6: Left (top) and right (bottom) oblique views of the outcrop showing the complex nature of the deposit. Natural sedimentary sequences can be quite complex with layers that are highly variable in thickness and lateral extent. Often, macroscopic layers, or 'units' are identified though sedimentological mapping with differences between the units reflecting changes in the local depositional environment, origin of the sediments, stream dynamics, or subsequent superposition of pedogenic processes. A close inspection of individual macroscopic units within the stratigraphic sequence at the Rio Bravo site reveals each unit to be composed of a hierarchy of many sub-unit layers. At small-scale, the bedding is composed of alternating fine-coarse layers obviously truncated by local erosion and re-deposition of sediments resulting in the superimposition of a variety of longer length scales that increase the variability within the macro-unit.

2.3 Site Development

Most of the effort to prepare the site involved leveling an infiltration surface in the indurated upper most unit (Unit 5). Additional site preparation involved setting up the garbage can water supply system and installing the infiltrometer.

Figure 2.7: Preparation of the infiltration surface. Karl Martin is creating a horizontal and flat infiltration surface on top of Unit 1. This unit is a calcium carbonate cemented sandstone and the most indurated bed in the outcrop. Note Bob Glass taking precise notes on Karl's pickaxe-operating technique which led to estimates of formation hardness calculated from Karl's apparent effort versus depth of penetration of the pick ax. The hardness was then converted to parameters commonly used to describe the relationship between saturation and matric potential which then is used to obtain an expression for the unsaturated hydraulic conductivity that then is used to simulate unsaturated flow. This method has been found to be at least as accurate and meaningful as measuring the same parameters on disturbed sediments in the laboratory with hanging columns (data yet to be published by R.J. Glass and J.R. Brainard).

Figure 2.8: Checking for a level infiltration surface. Karl Martin carefully checks for a level infiltration surface.

Figure 2.9: Infiltrometer installation. After the infiltration surface was leveled, a trench matching the bottom opening of the infiltrometer was excavated to a depth of 5 cm and backfilled with a 20% bentonite-sand mixture. Here, Karl Martin is pressing the infiltrometer into the backfilled trench to form a seal between the infiltrometer and the outcrop.

Figure 2.10: View of completed infiltrometer installation. The infiltration system consisted of a 30 gallon trash can used as a reservoir, 3/8 inch plastic water supply lines, and a 40 cm by 40 cm open-ended box formed with galvanized sheet metal, and evaporative cooler float valves to maintain a constant water level in the infiltrometer. Here, Drew Baird is making final measurements on the infiltration system while Karl Martin takes notes. Infiltration rates were obtained by converting manually measured water depths to volumetric flow through a trashcan-rating curve. Bob Glass, wary of Drew Baird with pointy objects in hand, observes from a safe distance and begins closing-in just in case Karl needs help defending himself.

Figure 2.11: Final adjustments to the infiltrometer infiltration system. Bob Glass and Karl Martin make final adjustments to the float valves while Drew Baird continues to take notes.

Figure 2.12: Inspection of infiltrometer. Bob Glass discusses the infiltrometer installation with Karl Martin while Jim Brainard looks on from the left trying his best to look important while Drew Baird heads for a drink…of water.

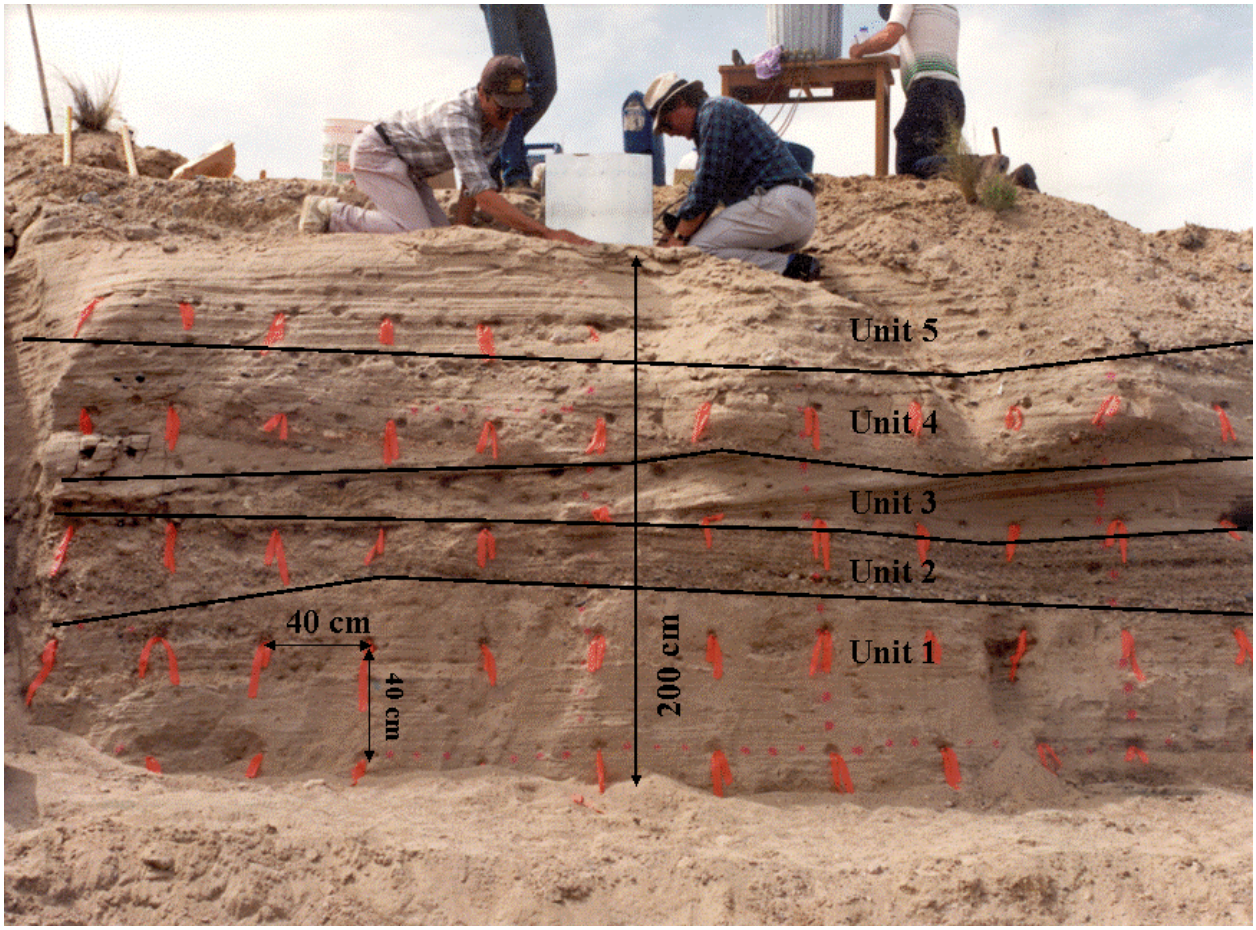

Figure 2.13: Layered fluvial outcrop at Rio Bravo. View of outcrop taken during the final stages of infiltrometer installation showing the contact locations of the five mapped units. The then youthful Bob Glass and Karl Martin are diligently installing the infiltrometer while Drew Baird records installation data in a field notebook. The legs belong to Jim Brainard. Note Drew Baird still taking notes.

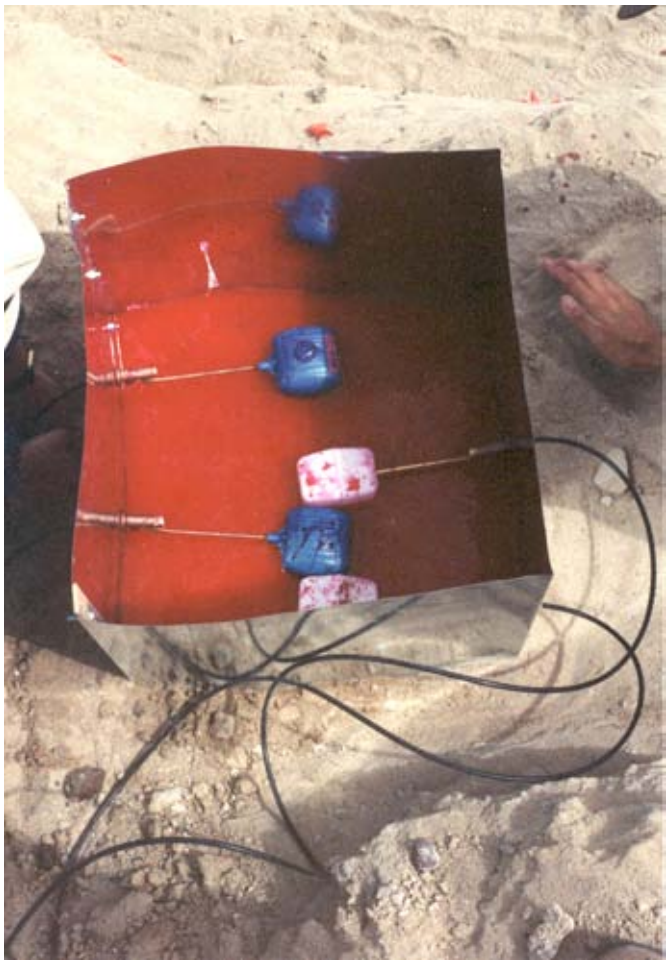

Figure 2.14: Top view of infiltrometer. The infiltrometer float valves can be seen in this photo. Infiltration was initiated by simultaneously dumping water into the infiltrometer and the trash can to provide an instant pond of water. Infiltration was initiated on May 9, 1992, with red dyed water supplied for the first 20 hours (370 liters) followed by a mix of green and blue dyed water lasting an additional 27 hours (549 liters). During this time, the infiltration rate was recorded by measuring the levels in the supply tank. Cameras located directly in front of the outcrop recorded the progression of the wetting front and development of the dye plume. Photographs were taken at regular intervals during daylight hours. Warner Jenkins Red Dye #3, Blue #1 and Green #3 which mixed at a concentration of 1g/l. At this concentration qualitative tests confirmed that the dyes adsorbed slightly to the sands and would lag behind the water. Does any one care for some punch minus the sugar, ascorbic acid and preservatives?

This page intentionally left blank.

3. Results

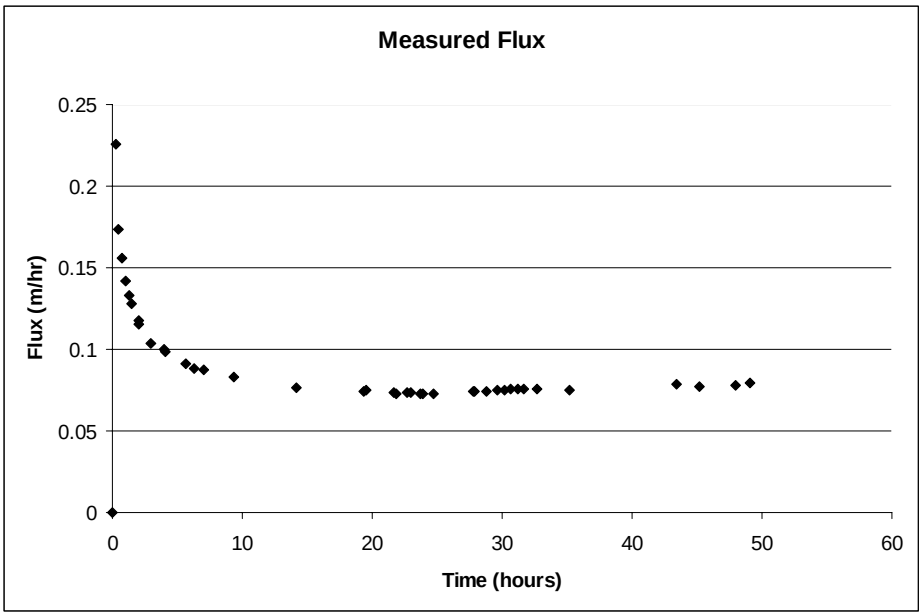

Figure 3.1: Experimental infiltration rate (m/hr) is plotted over the ~47 hour infiltration experiment. The observed infiltration rates follow the behavior of the standard infiltration equations/models [e.g., Kostiakov, 1932; Horton, 1933 and 1939; Green-Amp, 1911; Philip, 1969] where the initial infiltration rate drops to a constant rate over time. Initially the infiltration rate was near 0.23 m/hr and dropped to near 0.085 m/hr by 7 hours, and thereafter approached ~ 0.075 m/hr (Figure 4). The slight variations in the rate after 7 hours can be explained by the influence of temperature variation during the test on the viscosity of the infiltrating water. On the first day, the ambient maximum temperature was 23ºC. Over the following night and into the next day, temperature dropped to a minimum of 21ºC at the point where the infiltration rate had reached its minimum, then began to rise. On the last day of the experiment, the temperature had increased to 26ºC when the infiltration rate was 0.079 m/hr and slowly rising.

Figure 3.2: First Photo of developing bulb at 55 minutes. Within a few minutes of starting the infiltration, red dye appeared on the outcrop to the viewer's right side of the infiltrometer. The apparent asymmetry of the bulb at this early infiltration time is attributed to the drop off of the outcrop on the viewer's right side of the infiltrometer and not to formation heterogeneities. Drew Baird takes a well-deserved break from note writing while Bob Glass performs a little infiltrometer-formation seal maintenance and Jim Brainard ambles from left to right.

Figure 3.3: Developing bulb at 70 minutes. The bulb still appears to be asymmetric as it continues to expand down and out from the source.

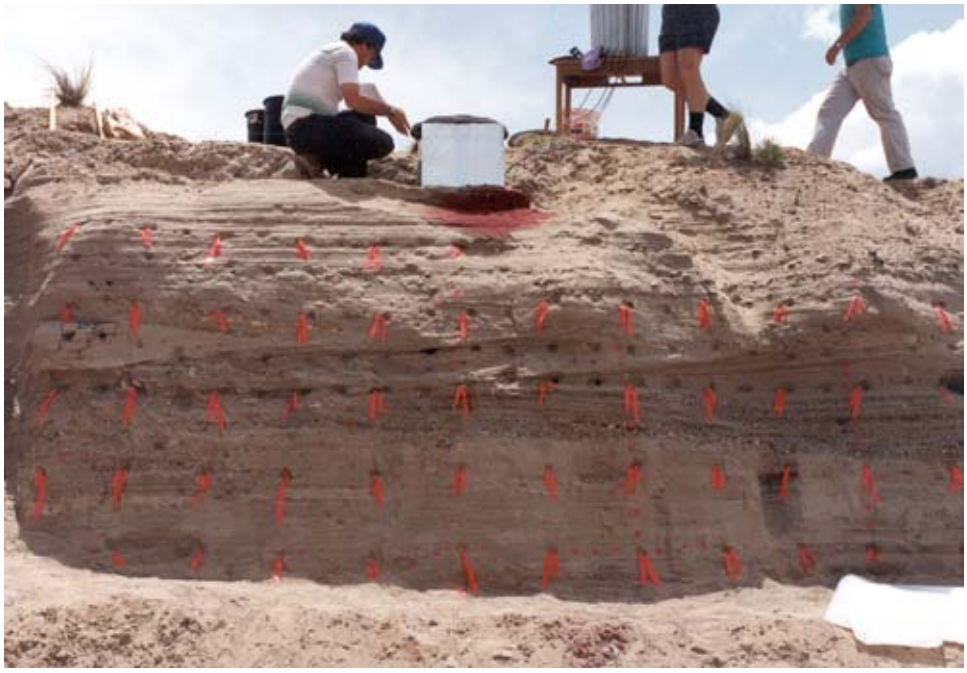

Figure 3.4: Developing bulb at 118 minutes. At this time the bulb appears to take on a more symmetrical shape while hints of dye absorption are becoming apparent as a clear water wetting front seems to be developing ahead of the dye plume. This is somewhat visible in the upper left part, and the lower most extent of the bulb. Notice the lid placed on the infiltrometer to minimize evaporation.

Figure 3.5: Developing bulb at 450 minutes. The outcrop was covered during the night to minimize impact from precipitation. At this time the bulb has expanded into an almost symmetric shape exhibiting considerable lateral spread and the wetting front has continued to move ahead of the dye front. Jim Brainard's then six year old Toyota is seen in the background. Now the Toyota is almost retired with nearly 300K miles on it…all on gas less than $1.50/gallon. Ah, the good old days!

Figure 3.6: Developing bulb at 1260 minutes. Close up of the bulb showing the red dye streamer emanating from the red dye bulb and extending to the wetting front along a fracture. The shape of the wetting front is also being influenced by the contact separating Unit 4 from the underlying Unit 3. Steep dipping cross-beds facing left can be seen in the sandstone below the contact in contrast to the pebble-sandstone above where the beds are dipping gently to the right. The lateral spread of the wetting front can be attributed to one of two flow mechanisms: ponding on top of a less hydraulically conductive bed or ponding on a capillary barrier. In the resistive bed case, the water would pond to a point where the water pressures would become positive and the hydraulic head (pressure gradient) would be sufficient enough to force the water through the more resistive bed. In the latter case, coarse over fine layers can create capillary barriers that promote lateral spread at the wetting front and eventual breakthrough with increasing moisture content and an associated increase –less negative- in water pressure (water pressure increases as water collects above the barrier allowing water to eventually move into the larger openings in the underlying coarser deposit). Since water was not observed to pour out of the outcrop, it is likely that a capillary barrier exists exactly at the contact where a thin fine bed occurs just above the contact between the two units.

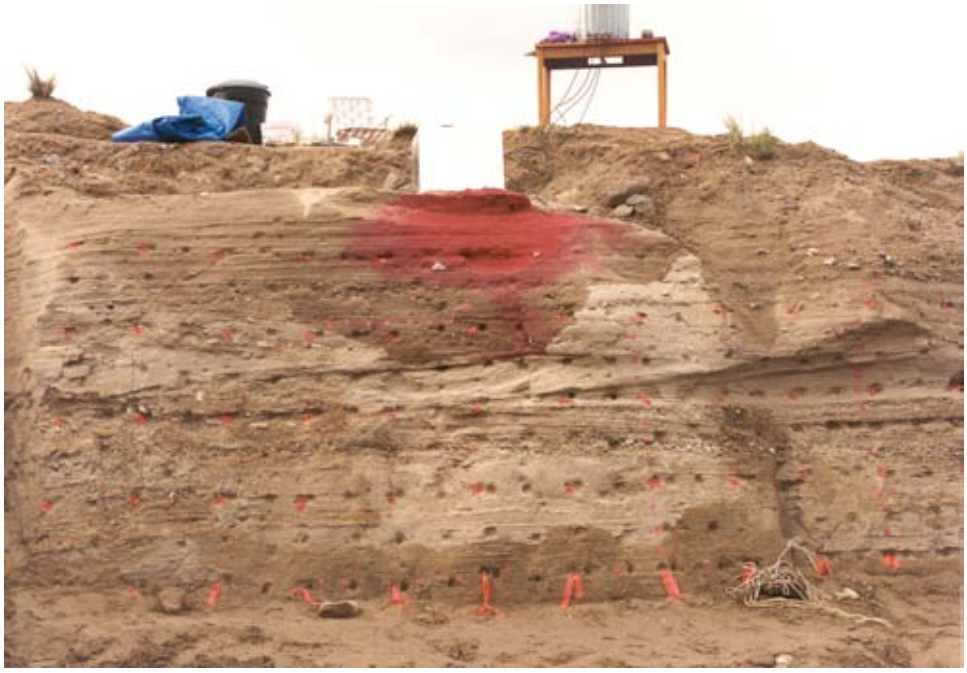

Figure 3.7: Developing bulb at 1336 minutes. The bulb has continued to expand laterally and downward and the wetting front continues to outpace the dye front. On the left side of the bulb, the wetting front is somewhat obliterated by the wet outcrop surface from the previous nights rain. The fracture continues to provide a fast pathway for the dye to the wetting front. The wetting front is now approaching a cut and fill contact within Unit 3, which may also be a capillary barrier. The blue-green dye tracer was started at 1200 minutes and is just slightly visible in this photograph as a darker red surface at the base of the infiltrometer.

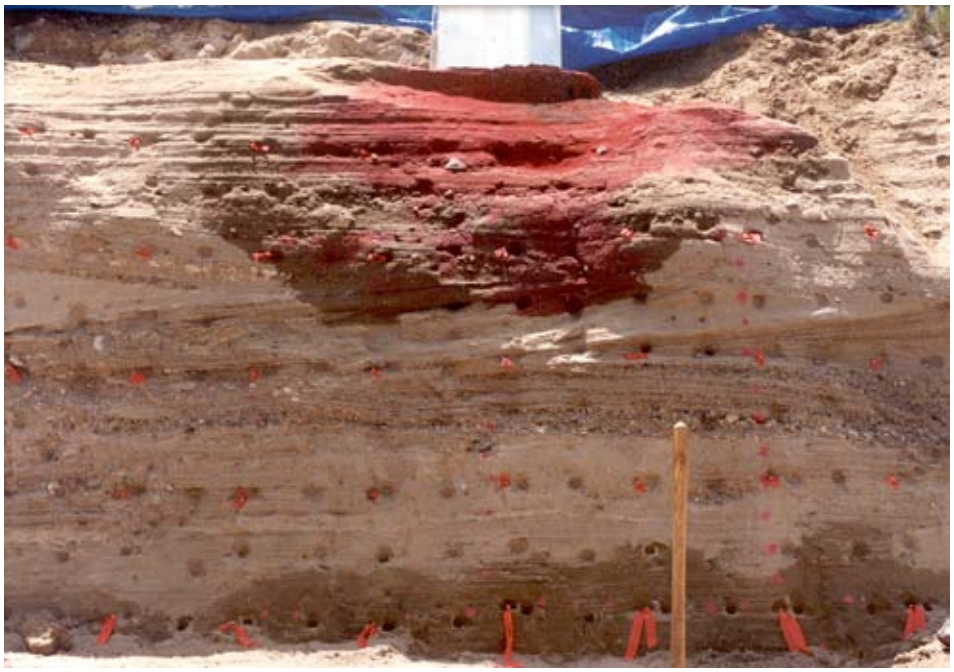

Figure 3.8: Developing bulb at 1675 minutes. In this vivid image, the wetting front is breaking through the suspected capillary barrier within Unit 3 and the apparent influences of the micro layering on the wetting front can be observed just below the barrier where flow appears to be occurring parallel to the cross-beds. The red dye plume is still lagging behind the wetting front and appears to be somewhat mottled in the bottom one-third of the bulb. The blue-green dye is now more apparent below the right side of the infiltrometer.

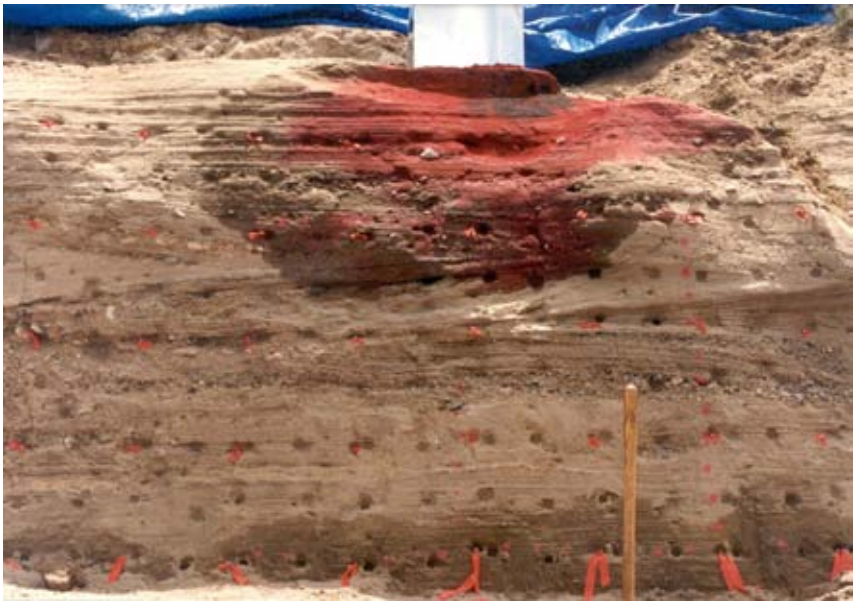

Figure 3.9: Developing bulb at 1740 minutes. The wetting front is progressing through the suspected capillary barrier within Unit 3.

Figure 3.10: Close up of wetting front breakthrough at a suspected capillary barrier at 1740 minutes. In this photo, the effects of small-scale layering on the wetting front are visible. It appears that the wetting front has moved through the suspected capillary barrier and then progressed preferentially laterally through finer grained beds.

Figure 3.11: Close up of wetting front at the left side of the bulb. At the side of the bulb, sequential capillary barriers promote horizontal flow.

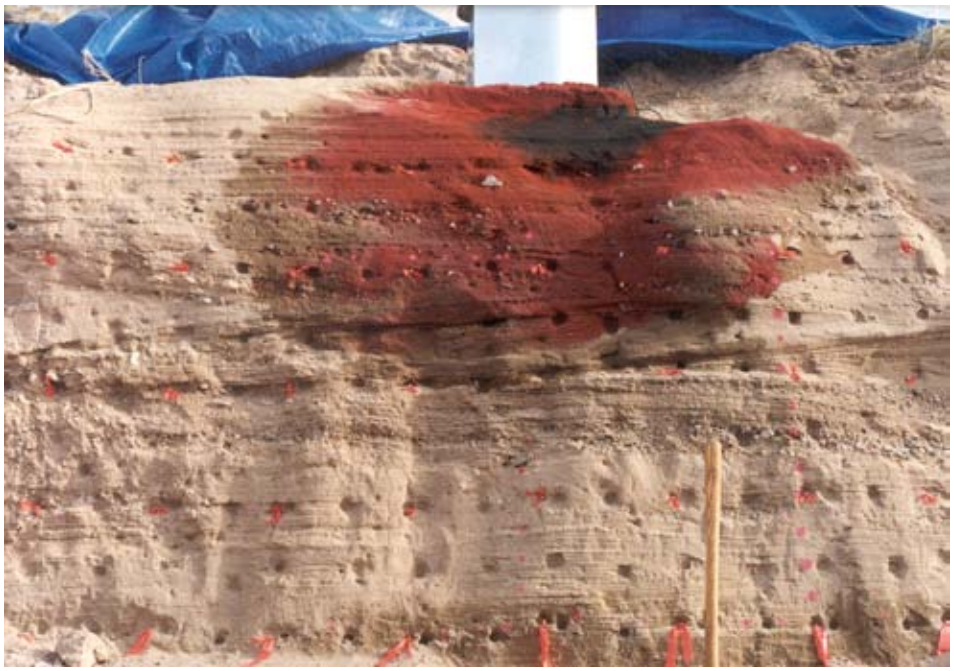

Figure 3.12: Developing bulb at 1905 minutes. The wetting front has passed a second capillary barrier and the apparent lag between the wetting front and red dye front seems to be diminished somewhat when compared to previous photographs. The mottling of the red dye bulb seems to be diminished compared to the previous photograph. The blue-green dye bulb is clearly evident in this photograph.

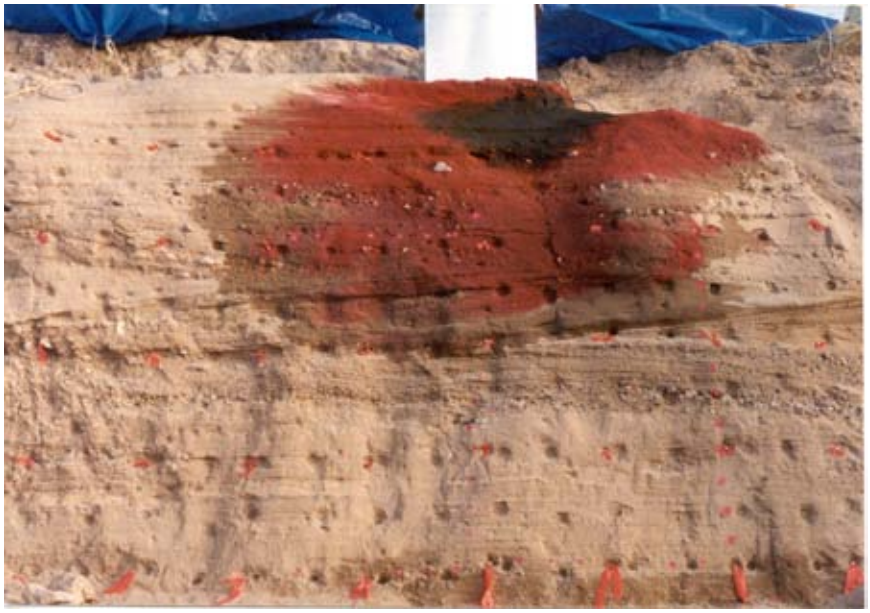

Figure 3.13: Developing bulb at 1960 minutes. Some small changes within the bulb can be observed when compared to the last photograph. In particular, the red bulb continues to loose its mottled appearance.

Figure 3.14: Developing Situation near 1960 minutes. A passing-by University of New Mexico art student stops to give a completely different interpretation of the dye plume.

Figure 3.15: Detachment of bulb from wetting front at 2110 minutes. An apparent detachment of the wetting front can be attributed to a third capillary barrier. This detachment occurs just above the contact between Unit 3 and the underlying Unit 2. The detachment is likely due to outward spread of the wetting front towards the outcrop surface similar to that observed in profile in Figure 3.11.

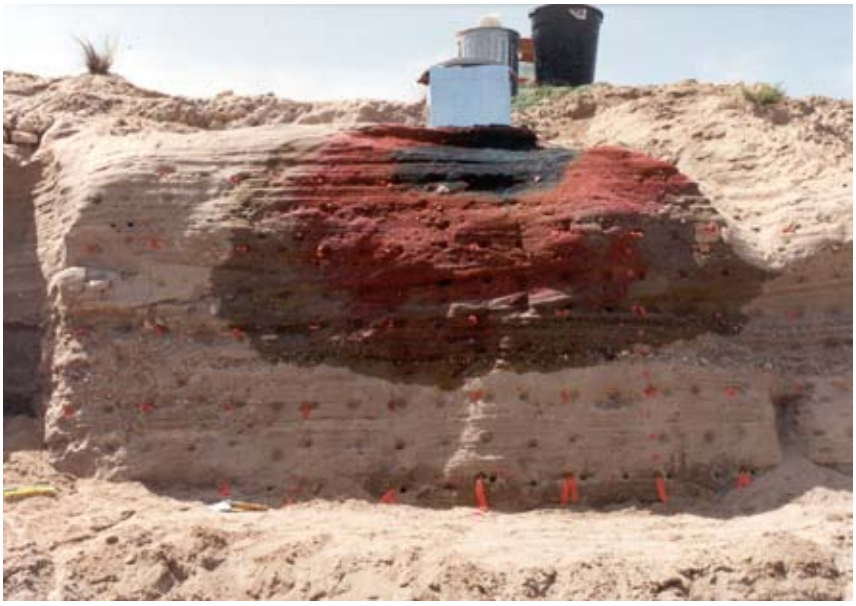

Figure 3.16: Developing bulb at 2890 minutes. In this photograph, the outcrop is not in direct sunlight which results in the appearance of a large separation of the red dye front from the wetting front. However, some vertical streamers can be seen extending below the wetting front and then spreading laterally. Also note the vertical line in the outcrop delineating the fracture mentioned earlier. It appears that the fracture has little influence on the flow field at this point.

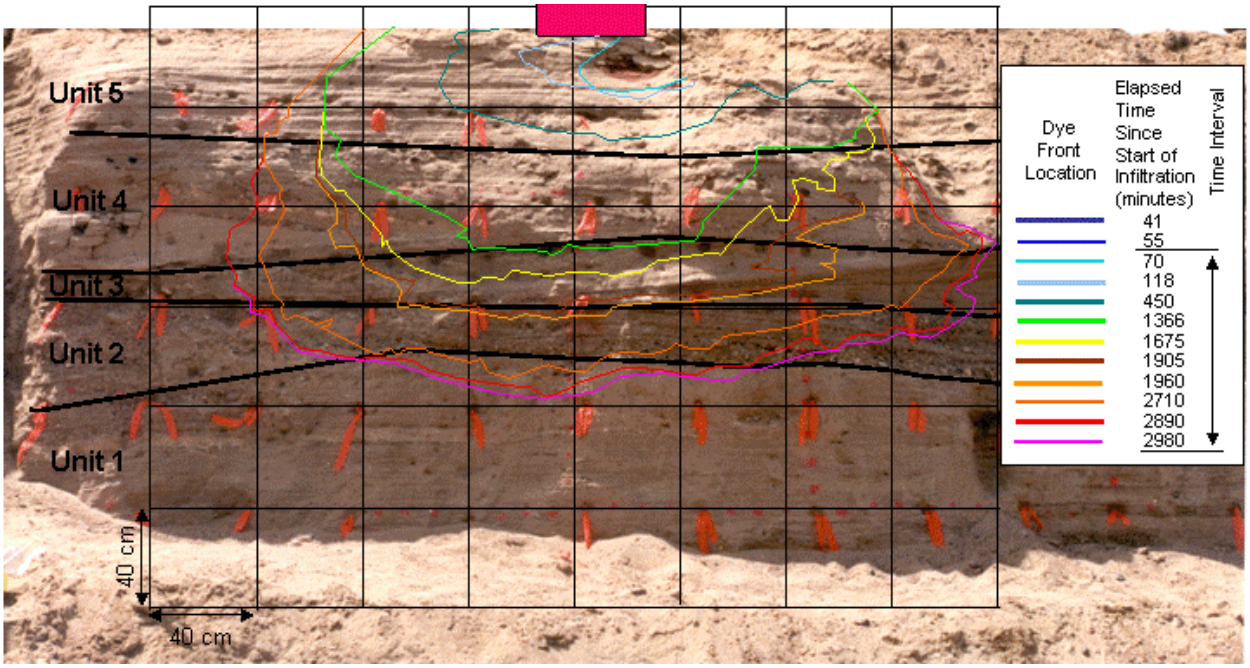

Figure 3.17: Two-dimensional plot of the clear water wetting front versus time. This and the following images were obtained directly from the photographs by digitizing the location of wetting and dye fronts from the previous photographs. Here, the position of the wetting front is presented along with the date, time and cumulative infiltration time. Despite the heterogeneities in the formation, the wetting front is fairly smooth but formed a bulb with a lateral extent twice the vertical.

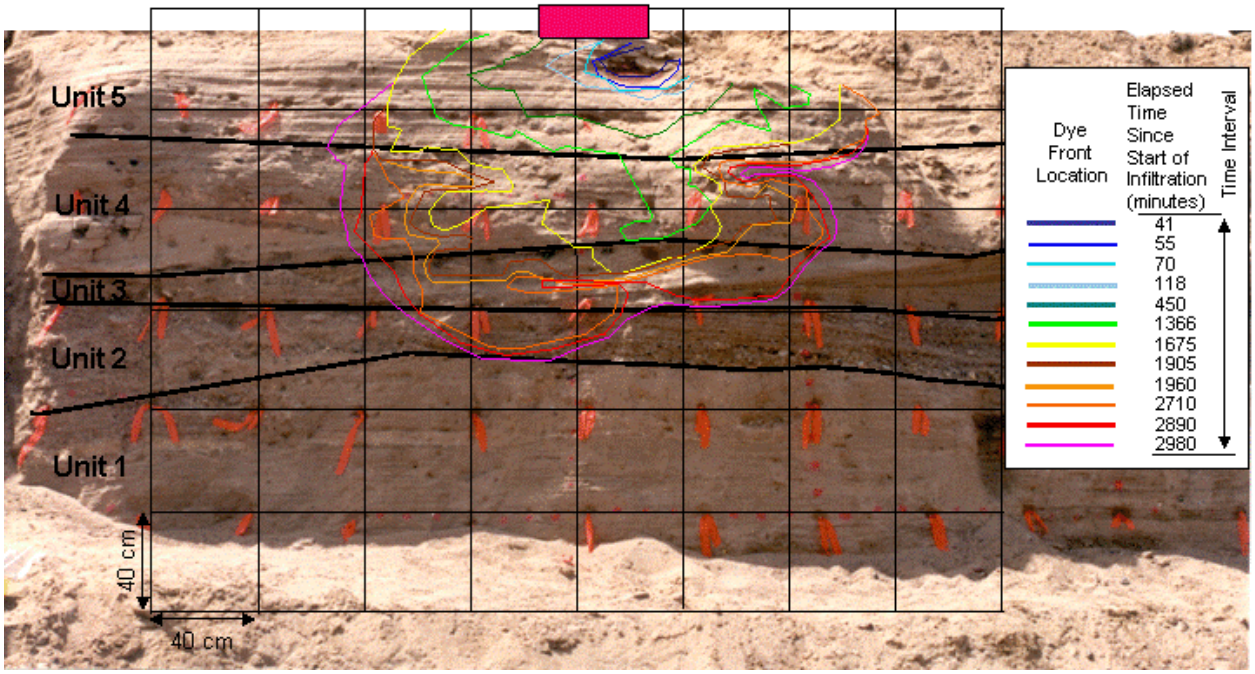

Figure 3.18: Two-dimensional plot of red dye front versus time. In contrast to the smooth wetting front, the red dye front exhibits a fairly complex pattern with deep embayments and peninsulas, some of which diminish with time and others that persist throughout the infiltration period.

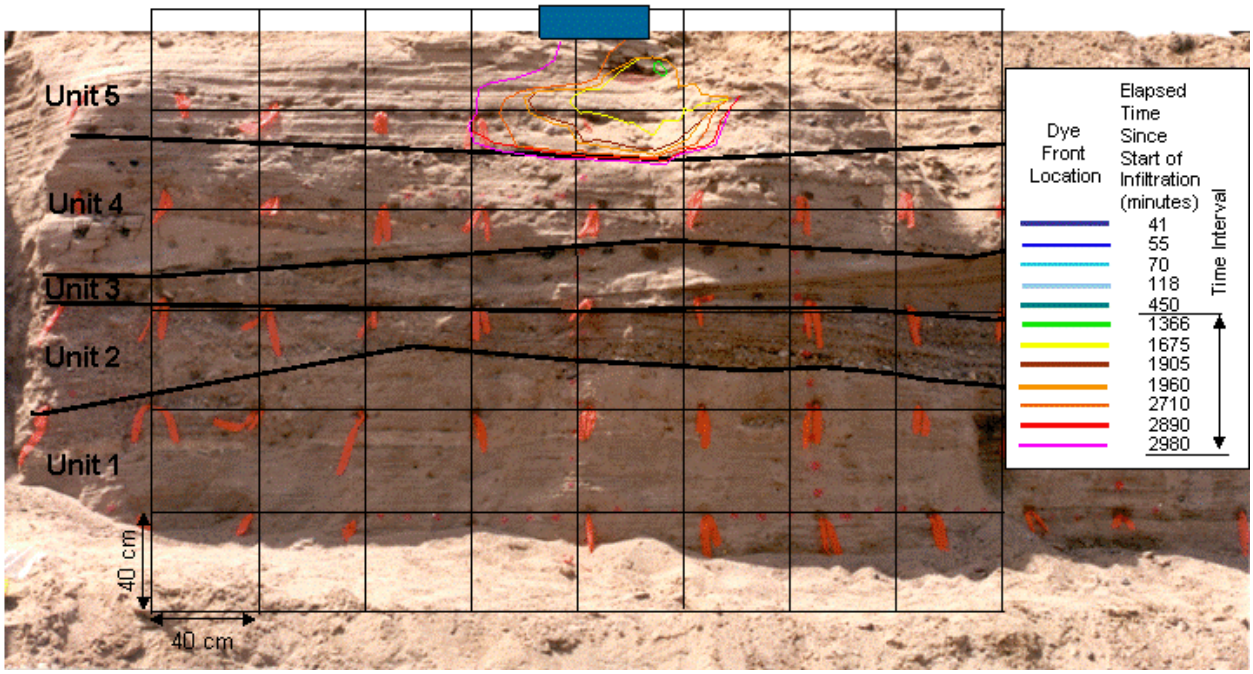

Figure 3.19: Two-dimensional plot of blue-green dye front versus time. The blue-green dye is plotted as a smooth boundary because the complexity of the fronts defied detailed reproduction. The time lines represent the best visual estimate of the blue-green dye front at the given times.

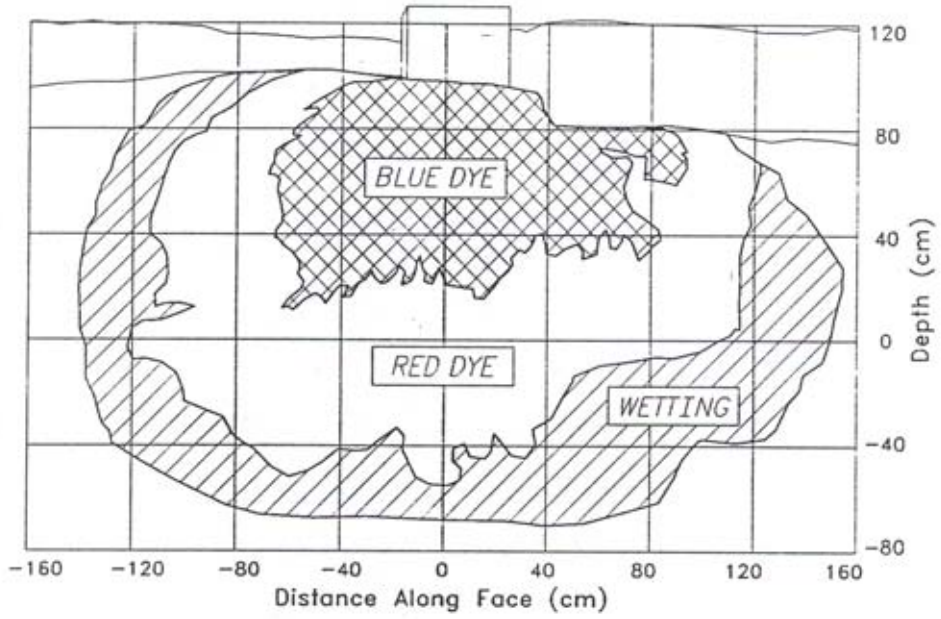

Figure 3.20: Composite drawings of water and red and blue fronts at the end of infiltration. The location of the three fronts in time for a) clear water or wetting, b) red dye, and c) blue-green dye.

4. Post-Infiltration Excavation

The next series of figures are photos and digital schematics of each face following excavation of slices from the outcrop face following the infiltration event. The excavated faces are exposed at 10-cm and greater intervals starting at the face and ending at the center of the infiltrometer. Notice in each of the photos the red and blue-green streamers radiating from the center of the plume.

Figure 4.1: First slice-70 cm from the center of the infiltrometer. The separation between the wetting front and the red dye front is pronounced and the three streamers in the red/clear water interface are large. Preferential horizontal spread of the wetting front along a select few layers can be seen on each side of the bulb as well as horizontal spread in the three large vertical red dye streamers. Notice the relatively smooth wetting front relative to the red dye/clear water front. A passerby provided the dog for scale.

Figure 4.2: Second slice-60 cm from the center of the infiltrometer. The photograph shows the first hint of streamer in the red/blue-green dye interface at the base of the blue-green dye bulb on the right hand side. This streamer is associated with the fracture seen in the photographs recording bulb development during infiltration. The red dye/clear water interface appears evenly distributed along the base of the red dye plum as compared to the previous photograph.

Figure 4.3: Third slice-50 cm from the center of the infiltrometer. In this photograph other dye streamers in the red/blue-green dye interface are approaching the length of the fracture streamer. The Red dye/clear water interface appears to contain some vertical streamers at the base of this interface and horizontal spread is observed in both the wetting front and the red dye plume along the sides.

Figure 4.4: Fourth slice-43 cm from the center of the infiltrometer. The non-fracture streamers become even more pronounced as the slices approach the infiltrometer. Localized horizontal spreading into a certain beds continues along the sides of the bulb in both the wetting front and the red dye plume. Vertical red dye streamers at the base of the red dye plume continue to be present.

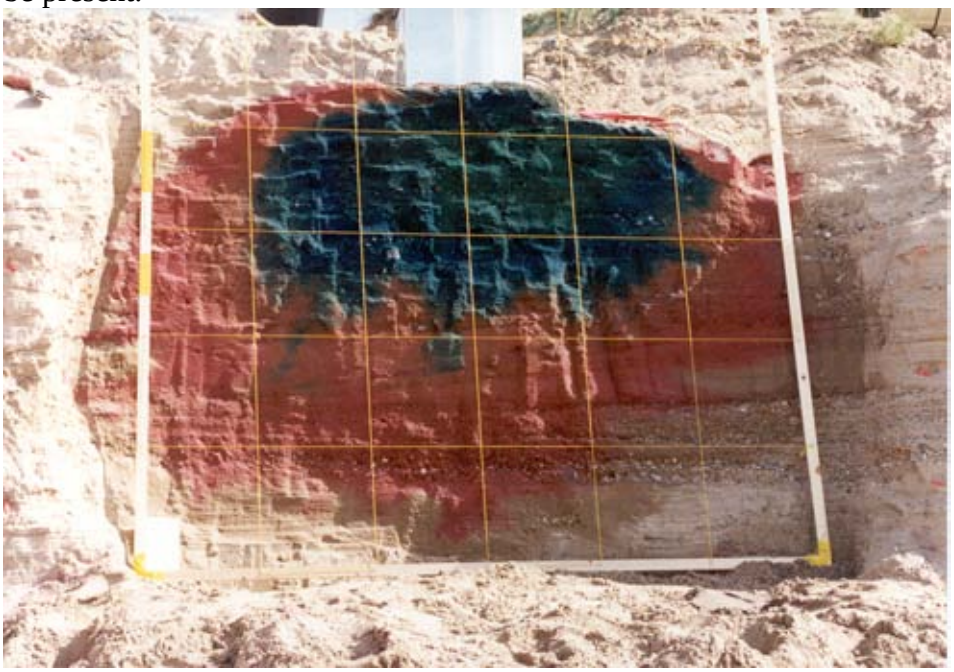

Figure 4.5: Fifth slice-37 cm from the center of the infiltrometer. Once again the dye streamer dominates the red/blue-green dye interface as most of the other streamers in this interface become less pronounced. Notice that some of the blue-green dye has traveled horizontally in a bed just left of the fracture streamer. Vertical streamers in the red dye are also observed. The 40 cm square grid is in place for mapping purposes.

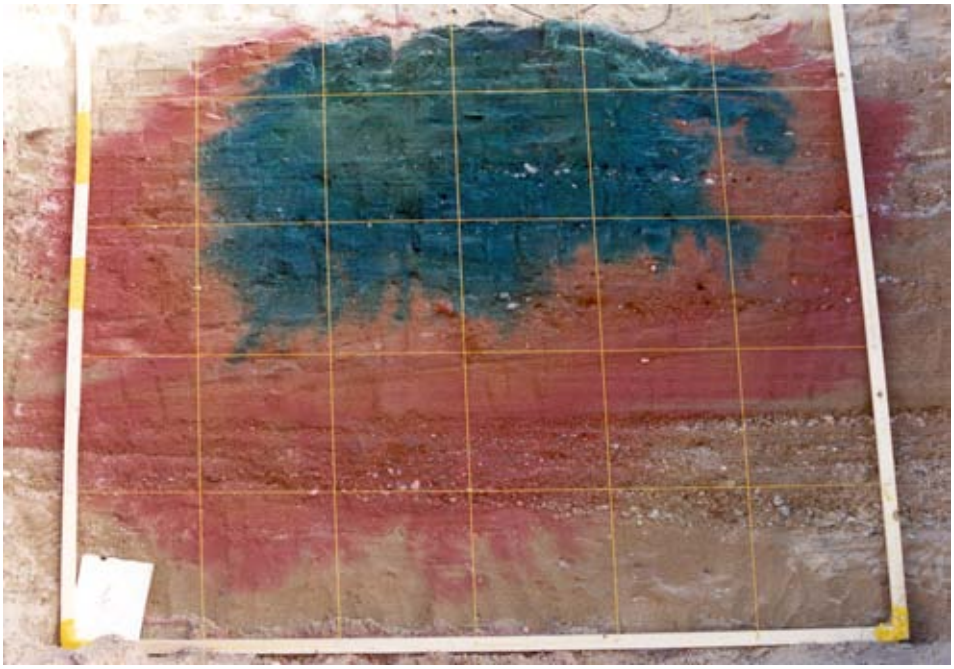

Figure 4.6: Sixth slice-at the center of the infiltrometer. This image shows many of the features identified so far in remarkable clarity. Notice that the fracture streamer is not readily apparent and the streamers appear to form independent of the stratigraphy by cutting across contacts without significant change in shape or size in most cases.

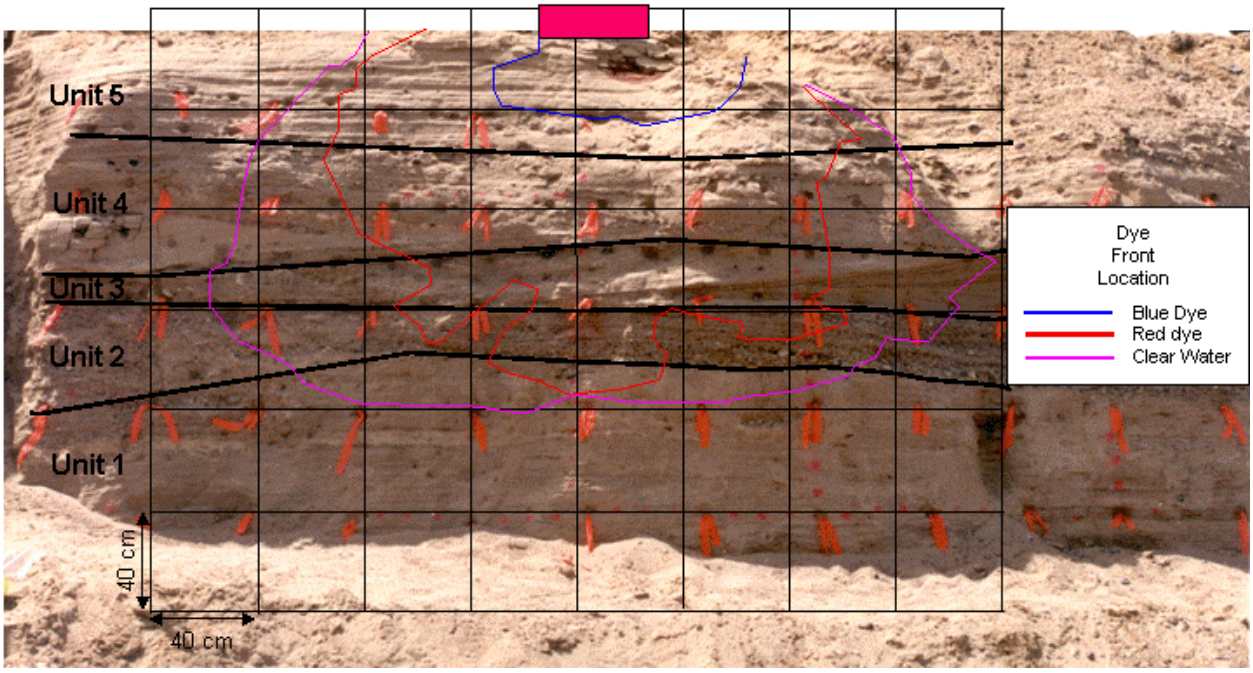

Figure 4.7: Schematic of Slice 1 (70 cm from the center of the infiltrometer) depicting the location of the blue-green, red and clear water front. The background is of the original outcrop shortly after the start of infiltration.

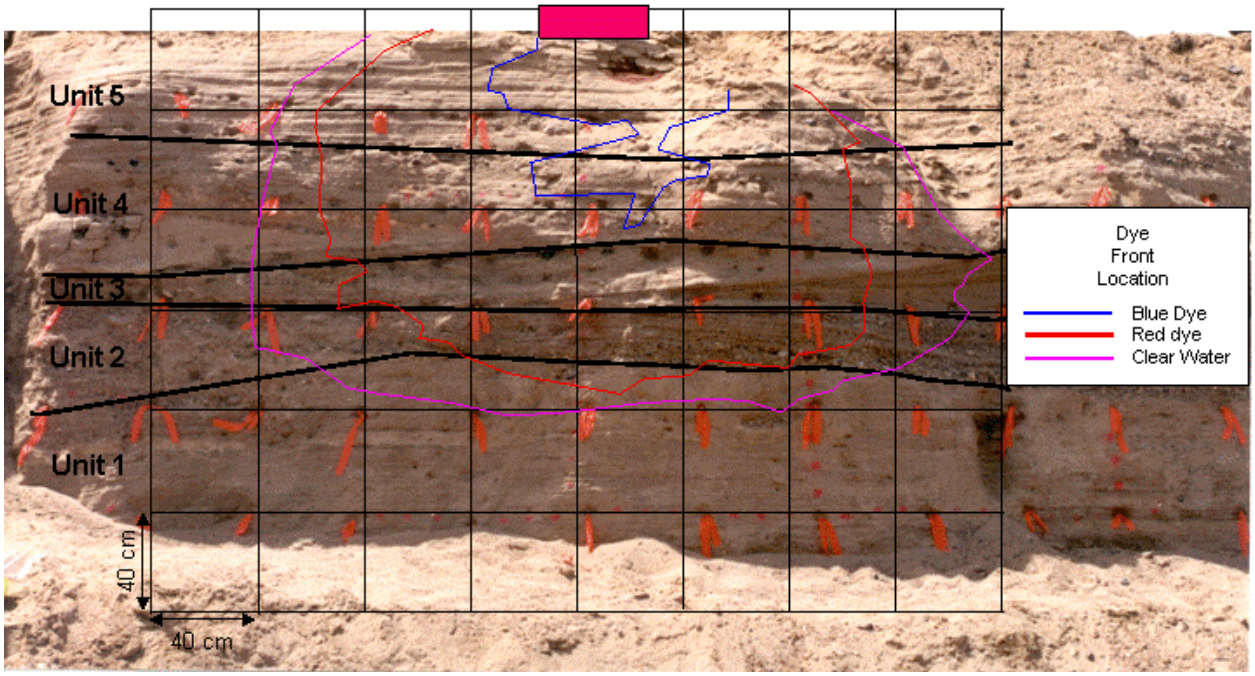

Figure 4.8: Schematic of Slice 2 (60 cm from the center of the infiltrometer) depicting the location of the blue-green, red and clear water front. The background is of the original outcrop shortly after the start of infiltration.

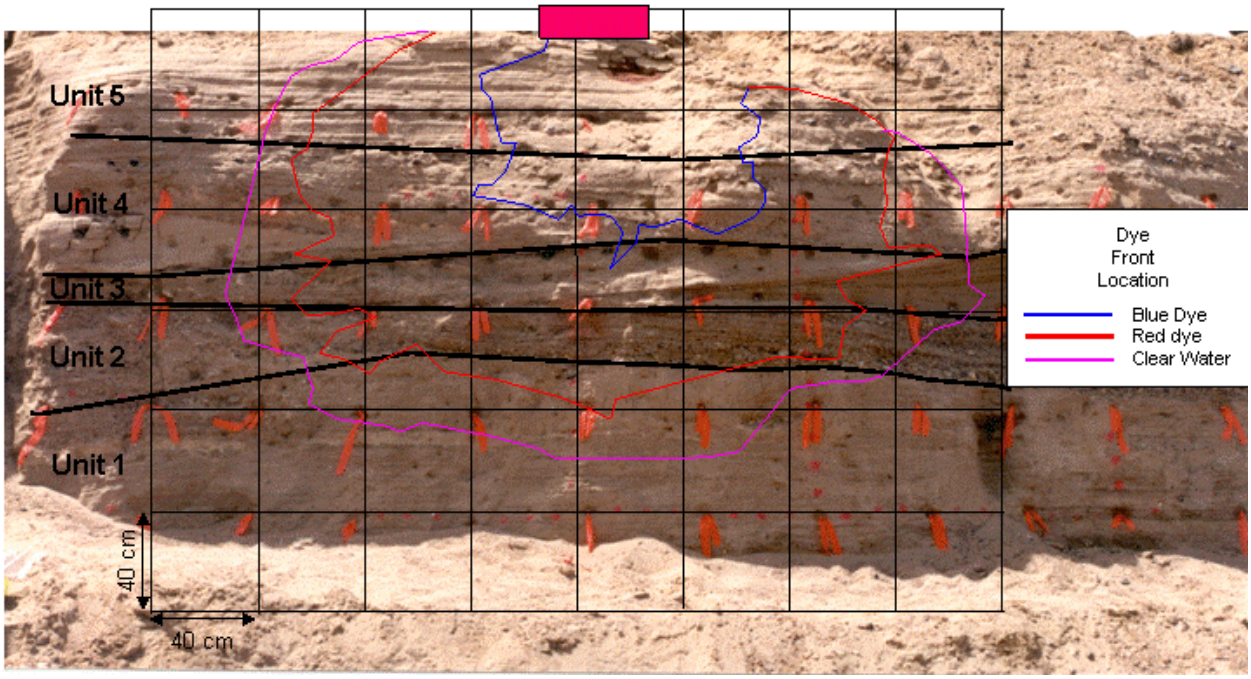

Figure 4.9: Schematic of Slice 3 (50 cm from the center of the infiltrometer) depicting the location of the blue-green, red and clear water front. The background is of the original outcrop shortly after the start of infiltration.

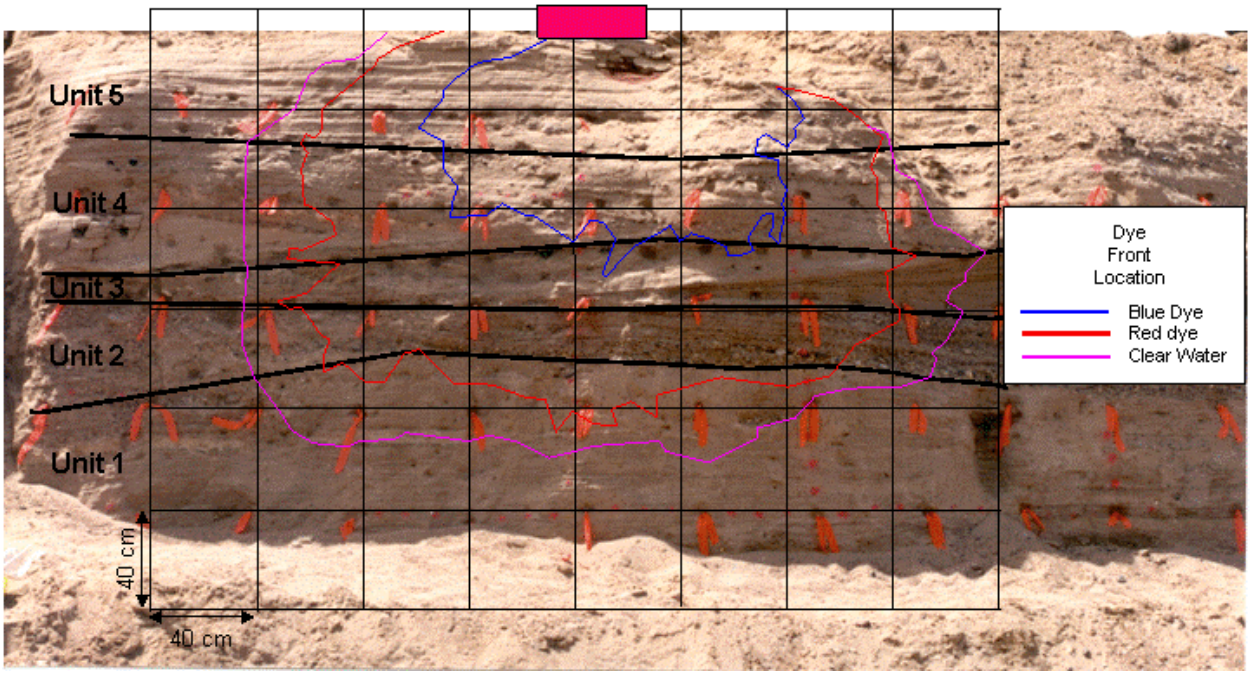

Figure 4.10: Schematic of Slice 4 (43 cm from the center of the infiltrometer) depicting the location of the blue-green, red and clear water front. The background is of the original outcrop shortly after the start of infiltration.

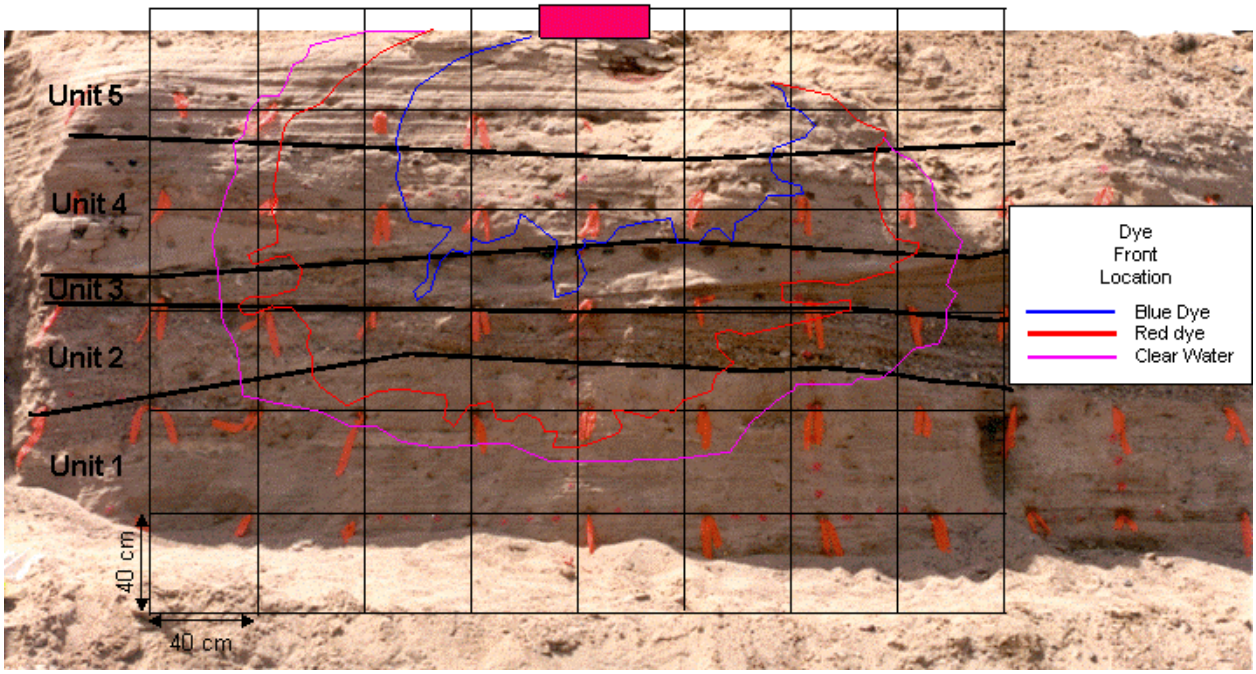

Figure 4.11: Schematic of Slice 5 (37 cm from the center of the infiltrometer) depicting the location of the blue-green, red and clear water front. The background is of the original outcrop shortly after the start of infiltration.

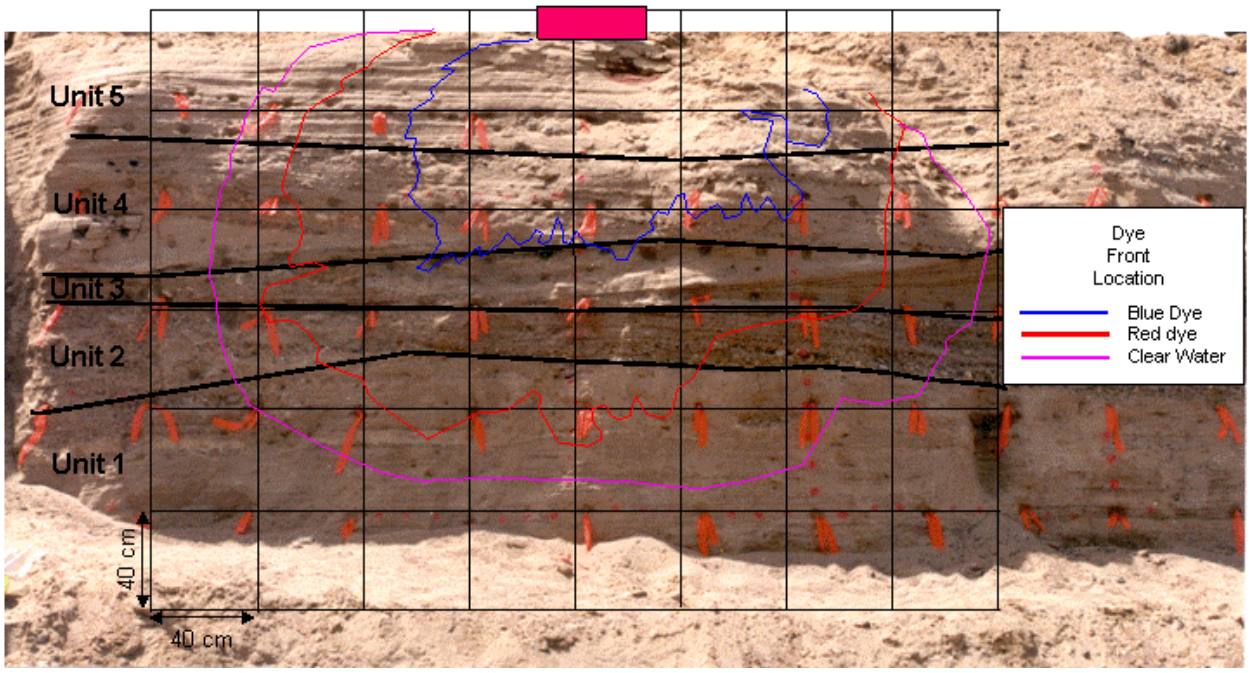

Figure 4.12: Schematic of Slice 6 (0 cm from the center of the infiltrometer) depicting the location of the blue-green, red and clear water front. The background is of the original outcrop shortly after the start of infiltration.

This page intentionally left blank.

5. Post Primary Excavation.

The following series of photographs were taken four months, one year, and three years after the initial excavation.

Figure 5.1: Undisturbed surface from the sixth slice four months after initial excavation. The basic shape seen in Figure 4.6 is preserved but note that the red and blue-green bulbs continued to expand, especially in the downward direction.

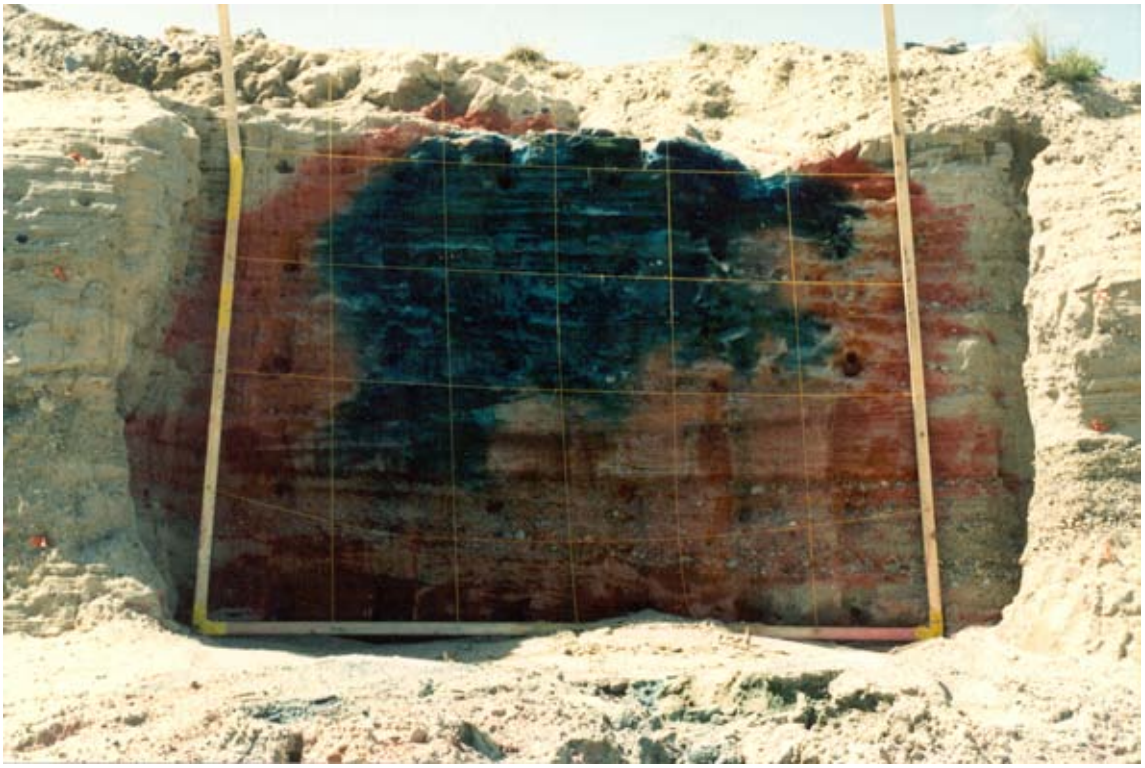

Figure 5.2 Excavated outcrop of Figure 5.1. Excavation revealed a pattern similar to Figure 5.1 and the photograph of the sixth slice (Figure 4.6) taken four months prior. Expansion of the dye plume is observed in this photograph also.

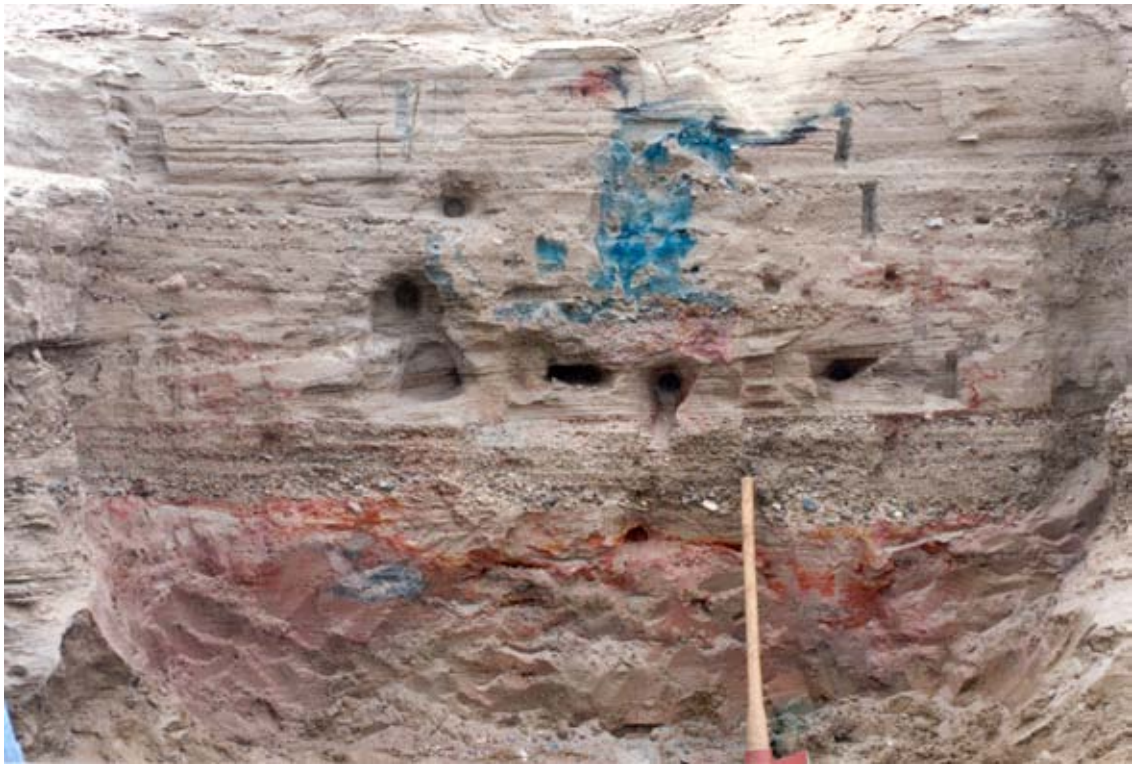

Figure 5.3: Partially excavated outcrop of Figure 5.2 one year after initial excavation. The blue in the center of the photograph is the remnant blue-green dye bulb while the red dye bulb appears significantly more faded. The original shape of either bulb cannot be discerned.

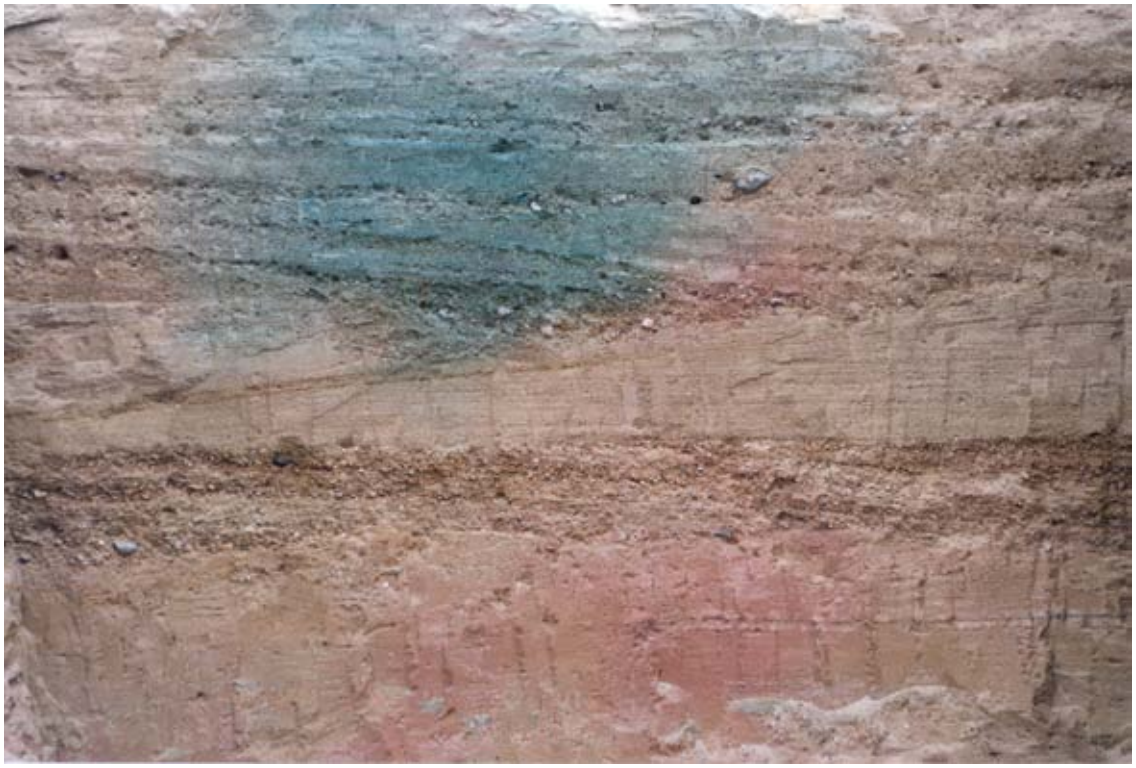

Figure 5.4: Fully excavated outcrop of figure 5.3. The blue-green bulb can be discerned easily while the red dye plume is significantly more faded. The original shape of the blue dye plume is almost identifiable, but the outer boundaries of the red dye plume are indistinct.

6. Concluding Remarks

The field experiment at the Rio Bravo site provided an excellent illustration of the spatial-temporal evolution of infiltrating water in a layered fluvial deposit. The deposit encompassed 5 mapped units each of which contained a multitude of smaller scale layers that ranged in thickness from several centimeters down to millimeters and had horizontal length scales ranging from several centimeters up to the width of our experiment and beyond. Yet, in this complex heterogeneous structure, a simple regular plume emerged. Small-scale irregularities at the wetting front averaged to yield a macroscopically smooth wetting front with significant anisotropy (lateral spreading ~ twice vertical).

Results at the Rio Bravo site also demonstrate that behind the wetting front, dye transport appears more heterogeneous and includes preferential movement directly to the front in context of crosscutting features (e.g., fractures). Because capillary pressure variability naturally decreases behind a wetting front, flow and thus advective transport behind the wetting front will be increasingly controlled by the differences in the hydraulic conductivity within the zone. In addition, movement of the dye will also be influenced if its adsorption varies in space. Regardless of whether variable flow (advection), variable adsorption, or some other process is responsible, the difference in structure between the wetting and dye fronts is interesting and begs for additional study in the future.

In conclusion, we emphasize that the infiltration experiment at the Rio Bravo sit was designed to be illustrative. Results show that the effect of layering is clearly significant in the natural fluvial deposit at the Rio Bravo site. Importantly, we found that for the advance of the wetting front, all the detailed small-scale behavior at the front averaged to produce a large-scale macroscopic symmetrical plume.

This page intentionally left blank.

7. References

Ababou, R., Three-dimensional flow in random porous media, Ph. D. thesis, Mass. Inst. of Technol., Cambridge, 1988.

Ababou, R., A. C. Bagtzoglou, B. Sagar, and G. Wittmeyer, Stochastic analysis of flow and transport, Chapter 6, in *Report on Research Activities for Calendar Year 1990*, Report NUREG/CR-5817, W. C. Patrick ed., U.S. Nuclear Regulatory Commission, Washington, D.C., 1991.

Alumbaugh, D., L.Paprocki, J.R. Brainard, R.J. Glass, and C. Rautman, Estimating initial moisture contents using cross-borehole ground penetrating radar: A study of accuracy and repeatability, *Water Resources Research*, 38(12), 1309, doi:10.1029/2001WR000754, 2002.

Bagnold, R. A., The physics of blown sand and desert dunes, Chapman and Hall, London, 265 pp., 1941.

Bagnold, R. A., The nature of saltation and of bed load transport in water, *Proc. R. Soc. A*, 332, 473-504, 1973.

Bagtzoglou, A. C., S. Mohanty, A. Nedungadi, T.-C. J. Yeh, and R. Ababou, Effective hydraulic property calculations for unsaturated fractured rock with semi-analytical and direct numerical techniques: Review and applications. CNWRA Report 94-007, Center for Nuclear Waste Regulatory Analyses, Southwest Research Institute, San Antonio, TX, 1994.

Binley, A, P. Winship, R. Middleton, M. Pokar, and J. West, High-resolution characterization of vadose zone dynamics using cross-borehole radar, *Water Resour. Res*, 37(11), doi:10.1029/2000wr000089, 2001.

Brainard, J. R., Vadose zone flow processes in heterogeneous alluvial fan deposits: experimental design, data evaluations, and error analysis, [M.S. thesis]: Department of Earth and Planetary Sciences, University of New Mexico, Albuquerque, New Mexico, 1997.

Brainard, J. R., R. J. Glass, D. L. Alumbaugh, L. Paprocki, D. J. La Brecque, X. Yang, T.-C. J. Yeh, K. E. Baker and C. A. Rautman, The Sandia-Tech Vadose Zone Facility: Experimental design and data report of a constant flux infiltration experiment, SAND Report, SAND2005-5070, Sandia National Laboratories, Albuquerque, New Mexico, 2004.

Flury, M., H. Flühler, W. A. Jury, and J. Leuenberger, Susceptibility of soils to preferential flow of water: A field study. *Water Resour. Res.*, 30(7): 1945-1954, 1994.

Gee, G. W., and A. L. Ward, Vadose zone transport field study: Status Report, PNNL-13679, Pacific Northwest National Laboratory, Richland, WA, 2001.

Ghodrati M., and W.A. Jury, A field study using dyes to characterize preferential flow of water. *Soil Science Society of America Journal*. 54: 1558-1563, 1990.

Glass, R.J. and M.J. Nicholl, Physics of gravity driven fingering of immiscible fluids within porous media: An overview of current understanding and selected complicating factors, *Geoderma*, 70:133-163, 1996.

Glass, R.J., M.J. Nicholl, A.L. Ramirez, W.D. Daily, Liquid phase structure within an unsaturated fracture network beneath a surface infiltration event: Field experiment, *Water Resour. Res.*, 38(10), 1199, doi:10.1029/2000WR000167, 2002.

Glass, R.J., T.S. Steenhuis and J-Y. Parlange, Wetting front instability as a rapid and far-reaching hydrologic process in the vadose zone, *Journal of Contaminant Hydrology*, 3(2-4):207-226, 1988.

Green, W. H. and G. A. Amp, Studies in soil physics. I. The flow of air and water through soils. *J. Agr. Sci.* 4:1-24, 1911.

Hawley, J. W., Guide Book to the Rio Grande Rift in New Mexico and Colorado, New Mexico Bureau of Mines and Mineral Resources, Circular 163, 1978.

Horton, R. E., The role of infiltration in the hydrologic cycle. *Trans. Am. Geophys.* Un., 14th Ann. Mtg., pp. 446-460, 1933.

Horton, R. E., Analysis of runoff-plot experiments with varying infiltration capacity. *Trans. Am. Geophys.* Un., 20th Ann. Mtg., Part IV., pp. 693-694, 1939.

Kelley, V. C., Geology of Albuquerque Basin, New Mexico, New Mexico Bureau of Mines and Mineral Resources, Memoir 33, 1977.

Kostiakov, A. N., On the dynamics of the coefficient of water percolation in soils and the necessity of studying it from a dynamic view for the purpose of amelioration. *Trans. 6th Congr. Int. Soc. Sci.*, Russian part A: 17-21, 1932.

Kung, K.J.S., Preferential flow in a sandy vadose zone, 1. Field Observation, *Geoderma* 46(1-3)51-58, 1990.

Martin, K.A., D.C. Baird, and R.J. Glass, Infiltration into thick unsaturated alluvial deposits: A preliminary study, *Proc. of the 1993 National Conf. on Hydraulic Engineering and International Symposium on Engineering Hydrology*, San Francisco, CA, July 25-30, 1993, Engineering Hydrology Volume, pp. 174-179, 1993.

McCord, J. T., D. B. Stephens and J. L. Wilson, Hysteresis and state-dependent anisotropy in modeling unsaturated hill slope hydrologic processes. *Water Resour. Res.* 27:1501-1518, 1991.

Nicholl, M.J., and R.J. Glass, Field investigation of flow processes in an initially dry fracture network at Fran Ridge, Yucca Mountain, Nevada: A photo essay and data summary, Sandia National Laboratories, Albuquerque, NM, SAND2002-1369, 2002.

Philip, J. R., 1969, The theory of infiltration. Adv. Hydrosci. 5:215-296.

Roepke, C., R.J. Glass, J. Brainard, M. Mann, K. Kriel, R. Holt and J. Schwing, Transport Processes Investigation: A necessary first step in site scale characterization plans, *Proceedings of Waste Management 95*, Feb 26 - March 7, Tucson, AZ, session 27, paper #20, 1995 (Sandia National Laboratories, Albuquerque, NM, SAND Report: SAND95-0289C, 1995).

Wierenga, P. J., L. W. Gelhar, C. S. Simmons, G. W. Gee, and T. J. Nicholson, Validation of stochastic flow and transport models for unsaturated soils: A comprehensive field study, Rep. NUREG/CR466-22, U.S. Nuel. Regul. Comm., Washington, D. C. Aug., 1986.

Yeh, T.-C. J., S. Liu, R. J. Glass, K. Baker, J.R. Brainard, D. Alumbaugh, and D. LaBrecque, A geostatistically based inverse model for electrical resistivity surveys and its applications to vadose zone hydrology, Water Resour. Res., 38(12), 1278, doi: 10.1029/2001WR001204, 2002.

DISTRIBUTION:

1	0735	J.R. Brainard 06313
1	1138	R.J. Glass 06326
1	8523	Central Technical Files
2	4414	Technical Library